Development of a Shallow Convolutional Neural Network for the Detection of Inferior Myocardial Infarction from ECG Signals

by

Tahsin Reasat

MASTER OF SCIENCE IN ELECTRICAL AND ELECTRONIC ENGINEERING

Department of Electrical and Electronic Engineering

BANGLADESH UNIVERSITY OF ENGINEERING AND TECHNOLOGY

January 2019

The thesis entitled **"Development of a Shallow Convolutional Neural Network for the Detection of Inferior Myocardial Infarction from ECG Signals"** submitted by Student Name: Tahsin Reasat, Student No.: 1015062242, Session: October, 2015 has been accepted as satisfactory in partial fulfillment of the requirement for the degree of MASTER OF SCIENCE IN ELECTRICAL AND ELECTRONIC ENGINEERING on January 2, 2019.

BOARD OF EXAMINERS

1. Celia Shahnaz

(Dr. Celia Shahnaz) **Chairman**
Professor (Supervisor)
Department of Electrical and Electronic Engineering
Bangladesh University of Engineering and Technology
Dhaka - 1000, Bangladesh.

2.

(Dr. Md. Shafiqul Islam) **Member**
Professor and Head (Ex-officio)
Department of Electrical and Electronic Engineering
Bangladesh University of Engineering and Technology
Dhaka - 1000, Bangladesh.

3.

(Dr. Mohammed Imamul Hassan Bhuiyan) **Member**
Associate Professor
Department of Electrical and Electronic Engineering
Bangladesh University of Engineering and Technology
Dhaka - 1000, Bangladesh.

4. Ahmad 02/01/2019

(Dr. Mohiuddin Ahmad) **Member**
Professor (External)
Department of Electrical and Electronic Engineering
Khulna University of Engineering & Technology Khulna - 9203, Bangladesh.

CANDIDATE'S DECLARATION

I, do, hereby declare that neither this thesis nor any part of it has been submitted elsewhere for the award of any degree or diploma.

Signature of the Candidate

Tahsin Reasat 05|01|2019

Tahsin Reasat

Dedication

To my parents.

Acknowledgment

I would like to express my sincere gratitude to my supervisor Dr. Celia Shahnaz for her guidance, encouragement, and support during the span of the research. I also want to thank her for inspiring me to explore new areas of research and spending a great amount of time to improve the write up of this dissertation.

I also like to thank the rest of the members of my thesis committee: Dr. Md. Shafiqul Islam, Dr. Mohammed Imamul Hassan Bhuiyan, Dr. Mohiuddin Ahmad, for their encouragement and insightful comments. I would like to thank the head of the Department of Electrical and Electronic Engineering for allowing me to use the lab facilities, which contributed greatly in completing the work in time.

Last but not the least, I would like to thank my parents, who raised me, supported me and taught me with utmost patience and love.

Abstract

Myocardial infarction (MI) is one of the leading causes of death around the world. MI can be diagnosed from the Electrocardiography (ECG) of the patient. The ECG is crucial for the patients survival in the early hours of MI as diagnosis from elevated serum cardiac enzymes takes 5-7 hours. This thesis presents a Convolutional Neural Network (CNN) architecture which takes raw Electrocardiography (ECG) signal from three ECG leads (lead II, III, AVF) and differentiates between inferior myocardial infarction (IMI) and healthy signals. A 5 layer deep network architecture consisting of inception blocks is developed. The discriminating strength of the features extracted by the convolutional layers by means of geometric separability index and Euclidean distance is analyzed and compared with the benchmark model. The performance of the CNN is also evaluated in terms of accuracy, sensitivity, and specificity and compared with the benchmark. The proposed model achieves superior metrics scores when compared to the benchmark model using hand engineered features. The detection models in the existing literature focused on ST segment elevation. But, studies showed that there is significant information in the leads containing ST segment depression. Hence, the IMI detection capability of different combinations of these leads needs to be investigated which is a computationally challenging task. We analyze the discriminating strength of the features extracted by the convolutional layers by means of geometric separability index and Euclidean distance and compare it with the benchmark model. Additionally, a comparison of the predictive capability (in terms of accuracy, sensitivity, and specificity) of different lead combinations is carried out. Experiments show that the combinations of leads that capture ST segment elevation and depression often outperforms the combinations of leads that capture ST segment elevation only.

Contents

List of Tables

List of Figures

List of abbreviations

ECG	Electrocardiogram
MI	Myocardial Infarction
IMI	Inferior Myocardial Infarction
AMI	Acute Myocardial Infarction
SWT	Stationary Wavelet Transform
CNN	Convolutional Neural Network
ANN	Artificial Neural Networks
SG	Savitzky-Golay
ReLU	Rectified Linear Unit
BN	Batch Normalization
MP	Max Pool
GSI	Geometric Separability Index
RNN	Recurrent Neural Network
DWT	Discrete Wavelet Transform
KNN	K-Nearest Neighbour
HC	Healthy Control
AIC	Akaike information criterion
HMM	Hidden Markov Model
GMM	Guassian Mixture Model
SVM	Support Vector Machine
VCG	Vectorcardiogram
RVM	Relevance Vector Machine
CWS	Complex Wavelet Sub-band

Chapter 1

INTRODUCTION

1.1 Introduction

Myocardial Infarction (MI), commonly known as 'heart attack', is the death of heart muscles (necrosis) due to prolonged lack of oxygen supply (ischemia). Myocardial infarction is the leading cause of death in the United States and in most industrialized nations throughout the world. In 2014, on average, someone in USA died every 4 minutes due to a stroke [1]. Survival rates improve after a heart attack if treatment begins within 1 hour. This signifies the necessity of accurate and timely diagnosis of MI.

1.1.1 Clinical Definition

A myocardial infarction is clinically defined as [2]:

- Elevated blood levels of cardiac enzymes (CKMB or Troponin T)

Additionally, one of the following criteria have to be met:

- The patient has typical complaints,
- The ECG shows ST elevation (Fig. 1.2) or depression.
- pathological Q waves develop on the ECG (Fig. 1.3)
- A coronary intervention had been performed (such as stent placement)

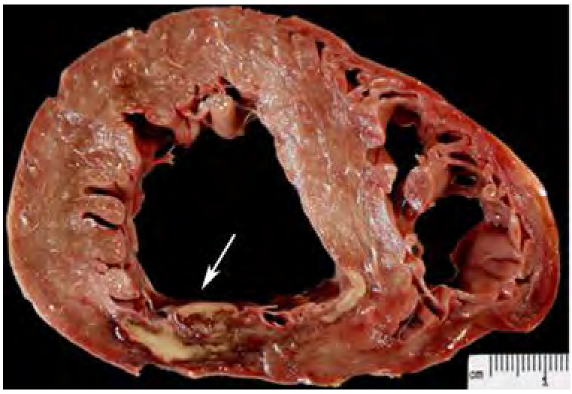

Figure 1.1: Acute Myocardial Infarction. At 3 days, there is a zone of yellow necrosis surrounded by darker hyperemic borders. The arrow points to a transmural infarct in the posterior wall of the left ventricle, in this short axis slice through the left and right ventricular chambers.

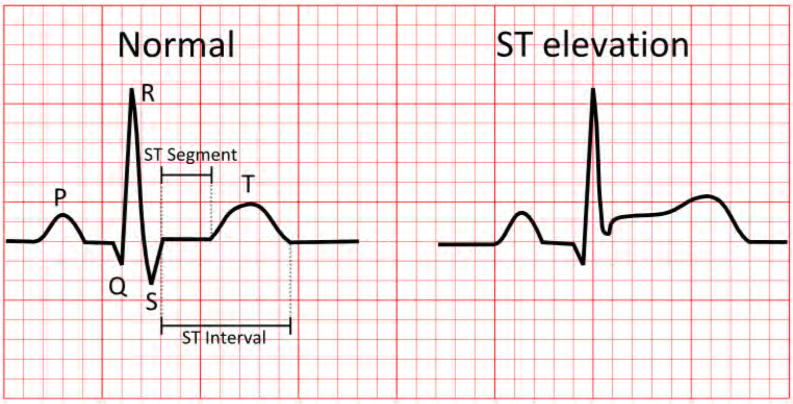

Figure 1.2: ST segment elevation due to MI.

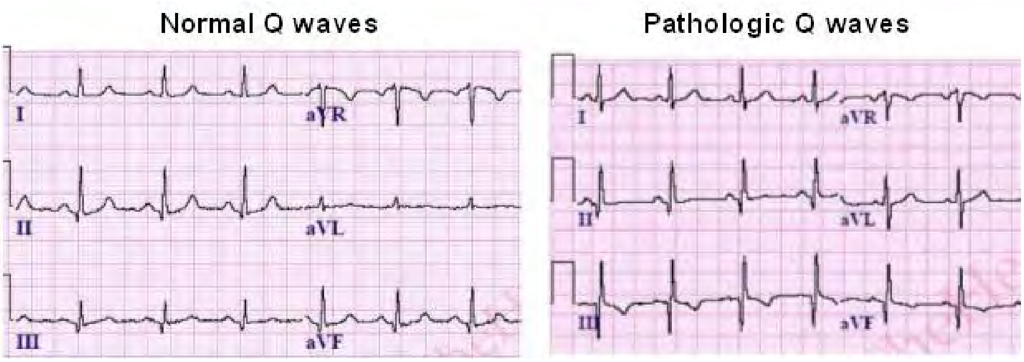

Figure 1.3: Pathological Q waves

1.1.2 Signs and symptoms

Patients with typical MI may have the following symptoms in the days or even weeks preceding the event (although typical STEMI may occur suddenly, without warning):

- Fatigue
- Chest discomfort
- Malaise

Typical chest pain in acute MI has the following characteristics:

- Intense and unremitting for 30-60 minutes
- Substernal, and often radiates up to the neck, shoulder, and jaw, and down the left arm
- Usually described as a substernal pressure sensation that also may be characterized as squeezing, aching, burning, or even sharp
- In some patients, the symptom is epigastric, with a feeling of indigestion or of fullness and gas

The patient's vital signs may demonstrate the following in MI:

- The patient's heart rate is often increased (tachycardic) secondary to a high sympathoadrenal discharge
- The pulse may be irregular because of ventricular ectopy, an accelerated idioventricular rhythm, ventricular tachycardia, atrial fibrillation or flutter, or other supraventricular arrhythmias; bradyarrhythmias may be present
- In general, the patient's blood pressure is initially elevated because of peripheral arterial vasoconstriction resulting from an adrenergic response to pain and ventricular dysfunction
- However, with right ventricular MI or severe left ventricular dysfunction, hypotension and cardiogenic shock can be seen

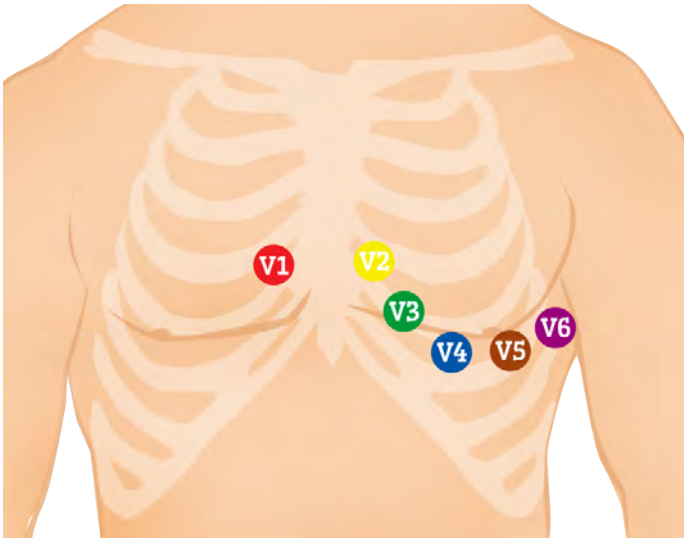

Figure 1.4: Placement of chest electrodes.

- The respiratory rate may be increased in response to pulmonary congestion or anxiety
- Coughing, wheezing, and the production of frothy sputum may occur

1.2 Use of ECG in MI detection

Although detection of elevated serum cardiac enzymes is more important than ECG changes, the cardiac enzymes can only be detected in the serum 5-7 hours after the onset of the myocardial infarction. Therefore, in the first few hours after the myocardial infarction, the ECG can be crucial. MI can be diagnosed by cardiologists based on the changes in the ECG, but the sensitivity and specificity of manual detection of acute MI is 91% and 51% as reported in [3]. Developing a computer aided system to automatically detect MI would help the cardiologists make better decisions. Before going in to the details of the relation between ECG leads and the location of MI, a detailed description of different electrodes and leads is given below.

1.2.1 Electrodes

In a 12-lead ECG, there are 12 leads calculated using 10 electrodes. The electrodes are divided in two categories. **Chest electrodes** and **Limb electrodes**. As shown in fig. 1.4, there are six chest electrodes.

1. V1 - Fourth intercostal space on the right sternum

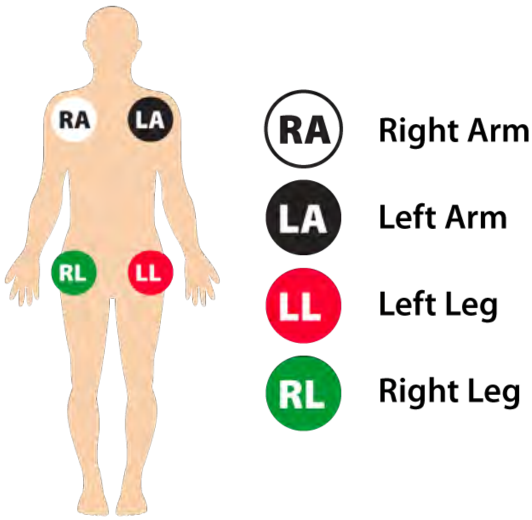

Figure 1.5: Placement of limb electrodes.

2. V2 - Fourth intercostal space at the left sternum
3. V3 - Midway between placement of V2 and V4
4. V4 - Fifth intercostal space at the midclavicular line
5. V5 - Anterior axillary line on the same horizontal level as V4
6. V6 - Mid-axillary line on the same horizontal level as V4 and V5

In addition to chest electrodes there are 4 limb electrodes (fig 1.5).

1. RA (Right Arm) - Anywhere between the right shoulder and right elbow
2. RL (Right Leg) - Anywhere below the right torso and above the right ankle
3. LA(Left Arm) - Anywhere between the left shoulder and the left elbow
4. LL (Left Leg) - Anywhere below the left torso and above the left ankle

1.2.2 Leads

A lead is a glimpse of the electrical activity of the heart from a particular angle. In 12-lead ECG, there are 10 electrodes providing 12 perspectives of the heart's activity using different angles through two electrical planes - vertical and horizontal planes.

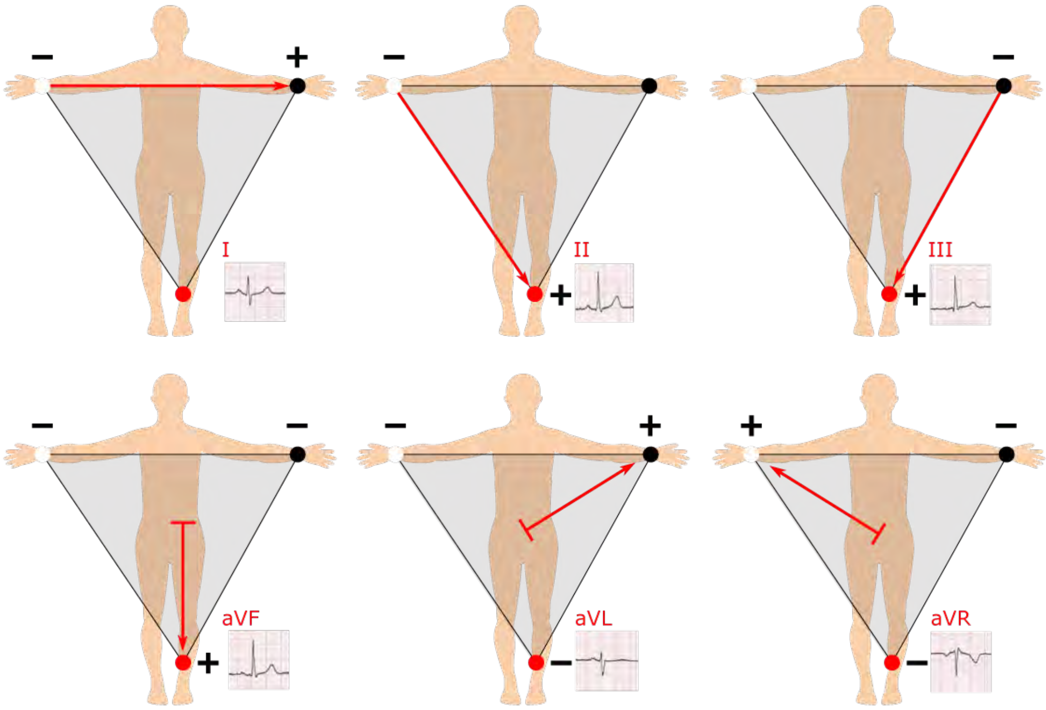

Figure 1.6: Einthoven's triangle.

Vertical plane (Frontal Leads)

By using 4 limb electrodes, we get 6 frontal leads that provide information about the heart's vertical plane:

1. Lead I
2. Lead II
3. Lead III
4. Augmented Vector Right (aVR)
5. Augmented Vector Left (aVL)
6. Augmented vector foot (aVF)

Leads I, II, and III require a negative and positive electrode (bipolarity) for monitoring. On the other hand, the augmented leads-aVR, aVL, and aVF-are unipolar and requires only a positive electrode for monitoring. The Einthoven's triangle (fig. 1.6) explains why there are 6 frontal leads when there are just 4 limb electrodes. The principle behind Einthoven's triangle describes how electrodes RA, LA and LL do

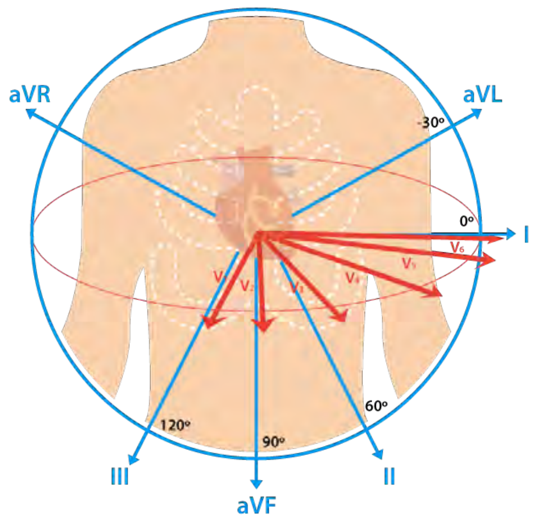

Figure 1.7: 12 leads showing 12 perspective of heart's electrical activity.

not only record the electrical activity of the heart in relation to themselves through the aVR, aVL and aVF leads. They also correspond with each other to form leads I (RA to LA), II (RA to LL) and III (LL to LA). As a result, they form an equilateral triangle. Hence it's called the Einthoven's triangle, named after Willem Einthoven who invented the first practical ECG.

Horizontal Plane (Transverse Leads)

By using 6 chest electrodes, we get 6 transverse leads that provide information about the heart's horizontal plane: V1, V2, V3, V4, V5, and V6.Like the augmented leads, the transverse leads are unipolar and requires only a positive electrode. The negative pole of all 6 leads is found at the center of the heart. This is calculated with the ECG.

1.3 Inferior Myocardial Infarction

Myocardial infarction can be classified according to the location of the infarct. Approximately 40% of all MIs involve the inferior wall (IMI) (Fig. 1.8). Traditionally, inferior MIs have a better prognosis than those in other regions, such as the anterior wall of the heart. The mortality rate of an inferior wall MI is less than 10%. However, a patient with inferior mycardial infarction should be sent for emergency cardiac angiography to the catheterization lab with a goal door-to-vessel open time of under 90 minutes [4]. Hence, fast and accurate detection of IMI is critical in a

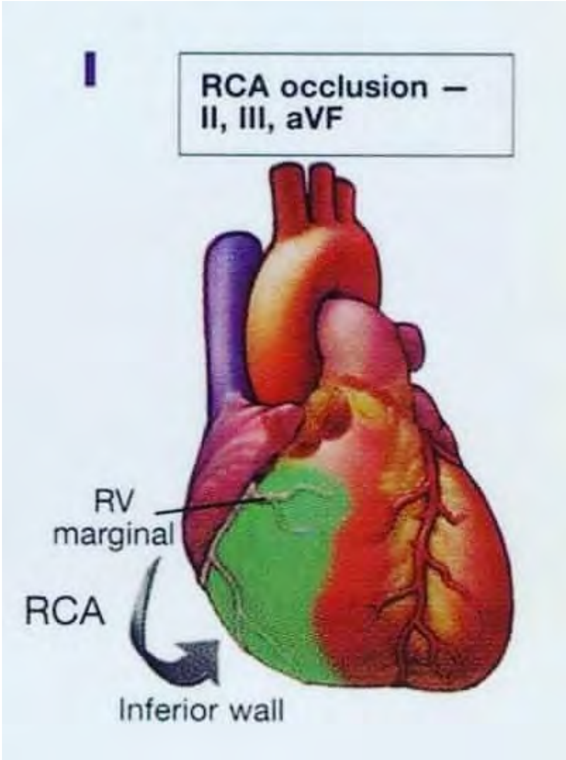

Figure 1.8: Inferior wall location of heart

patients survival.

1.4 Problem Definition

The ECG IMI detection task takes a set of ECG signal samples $\mathcal{S}$, consisting of simultaneous ECG signal segments of three different leads, as input, and outputs a label $y \in 0, 1$ for each of the elements of the set. Here, $\mathcal{S} = \{L_1, ...L_k\}$ where for each sample i, $L_k = \{x_i^p, x_i^q, x_i^r\}$. L represents the sample consisting of three leads, x represents the ECG segments, (p, q, r) are the three lead combinations where, $(p, q, r) \in \{I, II, III, V1, V2, V3, V4, AVF, AVL\}$

1.5 Motivation of finding most effective lead combination

In this thesis, we also focus on finding the three lead combination that performs best in detecting IMI. While developing IMI detection algorithms, prior researches have focused either on ECG leads II, III, and AVF (hereinafter, denoted as *reference lead combination*) or all of the 12 leads. Leads II, III, and AVF correlates with the inferior wall of the heart. ST segment elevation in those leads indicates an inferior wall ST elevation myocardial infarction (STEMI). However, if an electrocardiogram is obtained early enough it will often show ST segment depression in leads facing non-infarcting areas of the myocardium. Such ST depression has been called reciprocal and occurs in any or all of leads I, AVL and V1 to V6. [4]. According to researchers in [5] precordial ST segment depression during acute IMI is predictive of prognosis during and after hospitalization. Hence, it is also important to investigate the effect of the information included in the leads containing ST segment depression on IMI detection algorithms and find out the most effective lead combination.

1.6 Motivation of using Deep Learning

In the mathematical theory of artificial neural networks, the universal approximation theorem [6] states that a feed-forward network with a single hidden layer containing a finite number of neurons can approximate continuous functions on compact subsets of $\mathcal{R}^n$, under mild assumptions on the activation function. The theorem thus states that simple neural networks can represent a wide variety of interesting functions when given appropriate parameters; however, it does not touch upon the algorithmic learn ability of those parameters.

Keeping true to its property of being a universal function approximator, the neural networks and different variations of it have shown its effectiveness in different domains such as computer vision, speech recognition, natural language processing. Significant breakthroughs in complicated tasks like image classification, [7–10], object recognition [11, 12], segmentation [13–15] have been possible due to the utilization of neural networks.

In recent years, its application has quickly spread to many sectors including ECG signal. Convolutional neural networks (CNN) have been utilized in arrhythmia detection, coronary artery disease detection, beats classification, and biometrics [16–21]. Deep belief network has been used to classify signal quality in ECG [22]. Recurrent neural networks (RNN) have also been used in beats classification, obstruction of sleep apnea detection, ECG-based biometrics [23–25].

Due to the success of deep learning techniques in ECG signals, its use in MI detection is an interesting research direction. Earlier works in MI detection have taken a hand-crafted feature extraction approach for the classification problem. It would be convenient if the process of feature extraction/selection could also be automated. With this intention in mind, researchers have tried to borrow elements from *deep learning* and apply them to ECG signals. The key advantage of deep learning is that the model itself learns the most discriminative features from raw data and tries to match its output with the desired result.

1.7 Motivation of the thesis

The success of CNN's (e.g., in beat classification, rhythm classification etc.) in building an end to end model which takes raw ECG and produces the desired output without the help of any human intervention (feature engineering), has motivated us to investigate a CNN system which detects IMI from raw ECG signal and compare its performance with the state of the art feature based method. Since the ECGs signals are not complex in structure, performance of a shallow but wide CNN should be evaluated in IMI detection. Since the ST segment depression carries significant information of myocardial infarction it is necessary to investigate the predictive capability of different lead combinations which not only considers ST segment elevation but also ST segment depression.

1.8 Objective

In this work, we have investigated the performance of shallow CNN on the detection of IMI in a subject oriented approach along with the comparative analysis of the predictive capability of different lead combinations. The main contributions of this paper is listed below.

- To develop an end to end system to detect IMI from raw ECG signal and compare its performance with the state of the art feature based method.
- To design a shallow but wide CNN with less number of parameters compared to traditional deep CNNs.
- To evaluate the performance of the shallow CNN in a leave-one-patient-out (patient-oriented) approach and to make a qualitative comparison between

features extracted by the shallow CNN and the hand engineered features used in the current state of the art method.

- To investigate the predictive capability of different lead combinations which considers not only ST segment elevation but also ST segment depression.

The outcome of this thesis is the development of a shallow convolutional neural network based classifier which would automatically extract the relevant features from the raw ECG signal and detect IMI with greater accuracy, sensitivity, and specificity than the current state of the art methods. Additionally, the identification of the most effective lead combination to detect IMI is another significant outcome of this thesis.

1.9 Organization of the Thesis

This thesis is organized in the following way: Chapter 1 gives the introduction of the overall thesis. The problem statement and motivation behind the thesis in describe in this Chapter. In Chapter 2, literature review in MI detection is presented. Additionally the problems in the current approaches are discussed. In Chapter 3, the methodology is described in details. In Chapter 4, details regarding the simulations and the result analysis is presented. The conclusion is drawn in Chapter 5. Some interesting future research direction is also discussed in this section.

Chapter 2

LITERATURE REVIEW

2.1 Introduction

A vast number of research regarding MI detection from ECG has been done so far. A large portion of the research is been based on hand crafted features while there only a handful of research which involves deep learning. Hence, the previous works in ECG based MI detection can be primarily divided into two classes, hand engineered feature based approach and deep learning based approach.

2.2 Feature Extraction Based Approach

The feature extraction based approaches can be further classified into time-frequency domain based approach and only time domain based approach.

2.2.1 Time-Frequency domain based approach

The researchers in [26] have focused on a wavelet transform-based method. ECG signal obtained from 12 ECG leads were subjected to discrete wavelet transform (DWT) up to four levels of decomposition. Then, 12 nonlinear features namely, approximate entropy, signal energy, fuzzy entropy, Kolmogorov–Sinai entropy, permutation entropy, Renyi entropy, Shannon entropy, Tsallis entropy, wavelet entropy, fractal dimension, Kolmogorov complexity, and largest Lyapunov exponent were extracted from these DWT coefficients. The extracted features are then ranked based on the t-value. Then these features were fed into the k-nearest neighbor (KNN) classifier one by one to get the highest classification performance by using minimum number of features.

In [27], Stationary wavelet transform has been used to decompose the segmented multilead electrocardiogram (ECG) signal into different sub-bands. Sample entropy, normalized sub-band energy, log energy entropy, and median slope calculated over selected bands of multilead ECG are used as features. Support vector machine (SVM) and K-nearest neighbor (KNN) have been used to classify between subjects admitted for health control (HC) and patients suffering from IMI, using attributes selected on the basis of gain ratio.

In [28], researchers proposed a new deep feature learning based MI detection and classification approach. The model seeks to learn a representation of the extracted features (extracted from wavelet transforms) that optimize the classification performance. It incorporates multi-scale discrete wavelet transformation into the feature learning process to facilitate the extraction of MI features at specific frequency resolutions/scales.

2.2.2 Time domain based approach

In [29], time domain features of each beat in the ECG signal such as T wave amplitude, Q wave and ST level deviation, which are indicative of MI, were extracted from 12 leads ECG and used to detect MI.

Researchers in [30] proposed a novel ECG feature by fitting a given ECG signal with a 20th order polynomial function, defined as PolyECG-S. The PolyECG-S feature was almost identical to the fitted ECG curve, measured by the Akaike information criterion (AIC).

In contrast to the traditional approaches, [31] proposed a hybrid system with HMMs and GMMs which was employed for data classification. A hybrid approach using multi-leads, i.e., lead-V1, V2, V3 and V4 for myocardial infarction were developed and HMMs were used not only to find the ECG segmentations but also to calculate the log-likelihood value which was treated as statistical feature data of each heartbeat's ECG complex. The 4-dimension feature vector extracted by HMMs was clustered by GMMs with different numbers of distribution (disease and normal data). SVMs classifier was also examined for comparison with the proposed system.

In [32], MI pathology was detected using 12-lead ECG and vectorcardiogram (VCG). VCG is a method of recording the magnitude and direction of the electrical forces that are generated by the heart by means of a continuous series of vectors that form curving lines around a central point.VCG has the advantage to record the heart electrical activities in three orthogonal planes (frontal, sagittal and transverse). The researchers proposed a new method for automated detection or grading of MI pathology from vectorcardiogram (VCG) signals. The method used relevance vector machine (RVM) classifier and the multiscale features of VCG signal for MI detection. The multiscale analysis of VCG signal was performed using dual-tree complex wavelet transform. The diagnostic features such as the complex wavelet sub-band (CWS), L1 -Norm (CWS L1-norm) and the complex wavelet entropy (CWE) were evaluated from the sub-band complex wavelet coefficients of each orthogonal lead of VCG. The RVM classifier was considered to evaluate the performance of the combination of the CWS L1 -norm and the CWE features of VCG. Three different kernel functions such as Gaussian, bubble, and Cauchy were used for RVM.

In [33], artificial neural networks were trained to detect acute myocardial infarction by use of measurements from the 12 ST-T segments of each ECG, together with the correct diagnosis. After this training process, the performance of the neural networks was compared with that of a widely used ECG interpretation program and the classification of an experienced cardiologist. The neural networks showed higher sensitivities and discriminant power than both the interpretation program and cardiologist. However, this method needs accurate detection of some fiducial markers to extract the ST-T segment.

Researchers in [34] used artificial neural networks (ANNs) to detect signs of acute myocardial infarction (AMI) in ECGs. The 12-lead ECG was decomposed into Hermite basis functions, and the resulting coefficients were used as inputs to the ANNs. Furthermore, they presented a case-based method that qualitatively explains the operation of the ANNs, by showing regions of each ECG critical for ANN response. Key ingredients in this method are: (i) a cost function used to find local ECG perturbations leading to the largest possible change in ANN output and (ii) a minimization scheme for this cost function using mean field annealing.

However, all of these works reviewed thus far employ a hand crafted feature selection based approach. And there's always a chance that these hand crafted features may not the optimal set of features in IMI disease detection.

2.3 Deep Learning Based Approaches

At the time of writing this thesis there was only one research which used deep learning to produce a model that detected myocardial infarction from raw ECG data [35].

Although the model achieved satisfactory results on the experimental setup proposed in the paper, there are a few questions that remain to be asked. The researchers has implemented a *deep* network, however, it was shown that deep learners are not necessary for ECG signal analysis [18]. By downsampling the ECG signal, the researchers were able to train a shallow CNN and achieve superior results in beat classification. A shallow network requires fewer parameters and reduces training complexity. Hence, the performance of shallow CNN on MI detection needs to be evaluated. Hence, rather than creating a deep network a shallow but wide network might be more suitable for this sort of signals. The network layers in [35] have fixed kernel size in each layer. This might limit the networks scope for feature extraction because the optimal kernel size required for each of these layer ar not known. To compensate for that, an interesting approach is to create parallel layers of different sizes in at the same depth and take the aggregation of the activation/feature calculate by each parallel layer and propagate that forward. In essence, we are advocating a shallow but wide network in place of the deep but narrow network used in [35]. Another important aspect to take care is the partitioning of the data when conducting these experiments. The experiment in [35] was based on a *class-oriented* approach, i.e., heartbeats extracted from ECG signals were randomly sampled to form test and train set. As a result samples from the same patient contained in both test and train set. Therefore, it is not clear how the model will perform on patients it has never seen before. Hence, it is necessary to evaluate the performance of shallow convolutional neural networks on IMI detection using a subject-oriented approach. In this approach, the heartbeats are grouped according to the patients. The model is tested on heartbeats from one patient while it is trained on heartbeats from the rest of the patients. This procedure is repeated for the remaining the subjects.

2.4 Conclusion

In this Chapter, literature review on past researches on MI detection is performed. Some frequecny and time domain feature extraction based algorithms and their shortcomings have been discussed. Additionally, the only end to end deep learning based solution is discussed here. A few issues has been found in the deep learning based work which is addressed in this research. As discussed above, the presented deep learning model does not allow proper evaluation of its true potential due to data leakage in the train set. Hence, to test our model's generalization capability *subject-oriented* approach [27] is taken.

Chapter 3

DEVELOPMENT OF A SHALLOW CONVOLUTIONAL NEURAL NETWORK FOR THE DETECTION OF INFERIOR MYOCARDIAL INFARCTION FROM ECG SIGNALS

3.1 Introduction

Deep convolutional neural networks were originally designed to work on images. Each layer of a CNN extracts complicated features from images and each subsequent layer represents a complicated representation of the previous layer. Since an image is a two dimensional data and rich with complex characteristics, a deep network seems logical and works well in application. On the other hand, ECG is a one dimensional signal and not as characteristically rich as an image. Hence, a shallow CNN might be better off when analyzing ECG. This phenomenon has been shown by the researchers in [18] while performing beat classification. By downsampling the ECG signal, the researchers were able to train a shallow CNN and achieve superior results in beat classification. Shallow networks require fewer parameters which reduces training complexity. Inspired by their findings, we have developed a shallow CNN for IMI detection. In this Chapter, we describe the network architecture and our methodology.

3.2 Methodology

3.2.1 Overview

The signals from ECG leads are denoised using median filters and Savitzky-Golay (SG) smoothing filters (Fig. 3.1) and segmented into samples. Next, the samples are fed into the neural network architecture (Fig. 3.3b, Fig. 3.3a) and features are extracted to measure and compare their quality with the benchmark method. Additionally, the proposed model is trained and tested in a subject oriented approach and its performance is compared with the benchmark method. Finally, experiments on different combinations of leads are performed to find out the most effective lead for IMI detection. The details of the procedure are described in the following subsections.

3.2.2 Data Processing

As shown in Fig. 3.1, each signal is downsampled from 1kHz to 250Hz. A two stage median filter is used to remove baseline wandering. Next, Savitzky-Golay (SG) smoothing filter is used to remove noise. Up to this point the preprocessing steps are identical to [27]. The denoised signal is further downsampled to 64Hz to decrease computational burden on the convolutional network and speed up training time. Finally, the signals are partitioned into short segments of 3.072 seconds (196 signal samples per segment). The segments generated simultaneously from three different leads are grouped together to create a sample.

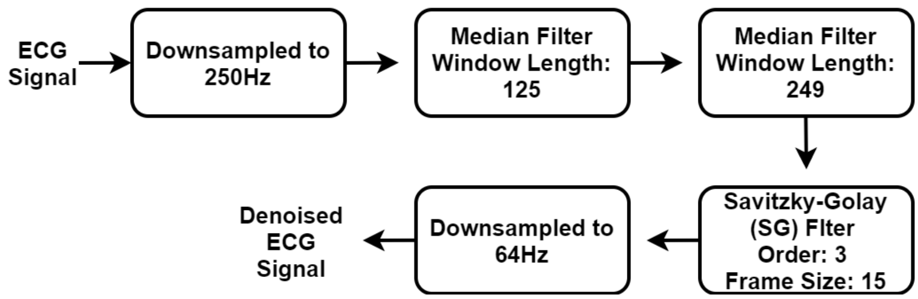

Figure 3.1: Data preprocessing

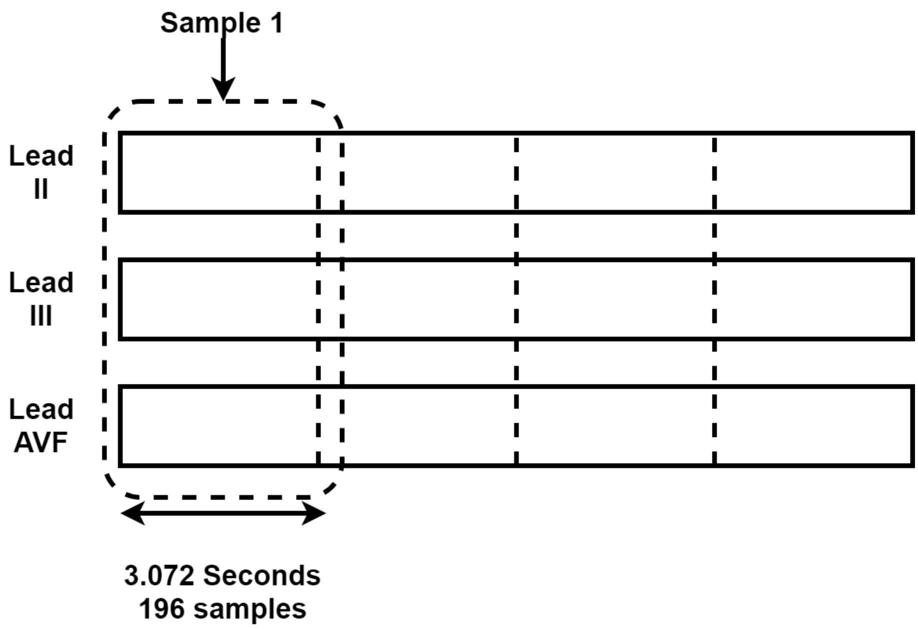

Figure 3.2: Data segmentation

3.2.3 Network Architecture

We implement a shallow but wide CNN whose architecture is inspired by the inception module in GoogleNet [36]. The high-level architecture of the model is illustrated in fig. 3.3a. The network takes raw ECG sample at the input layer. Each sample consists of signal segments from three leads, leads e.g., II, III and AVF. Each lead is fed into an *inception block* (fig. 3.3b). In the inception block, the input goes through seven parallel paths. In each parallel path, there is a convolutional layer followed by a batch normalization layer, a rectified linear unit (ReLU) activation layer and a max pooling layer. Feature maps extracted by the inception blocks are concatenated and passed on to a global average pooling layer. Finally, there is a 2 unit dense layer with a softmax activation layer which gives the categorical probability. The weight of the dense layer is L2 regularized to prevent it from overfitting. The motivation behind the structure of the key layers are described below.

Convolutional Layer

The function of the convolutional layer is to extract features from the input. In traditional CNNs, the filters of a particular layer have the same window length which is gradually reduced in the subsequent layers [37]. However, there are no hard and fast rules to select the window length and it is selected experimentally.

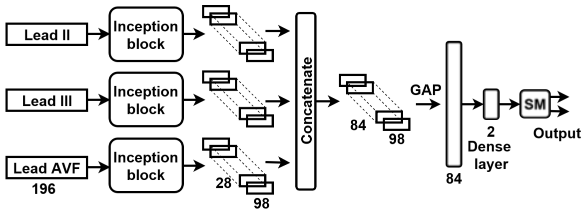

(a) The model architecture. Here GAP stands for Global Average Pooling and SM stands for Softmax.

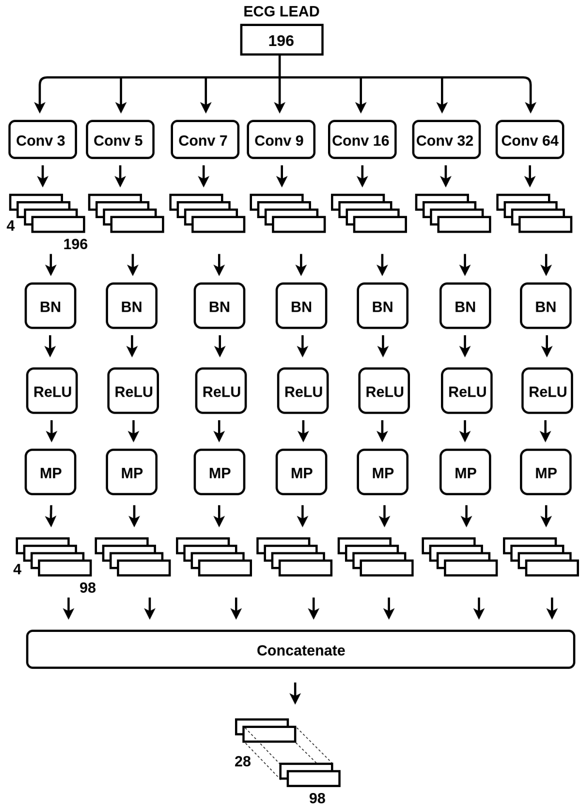

(b) The inception block. Each 'Conv n' layer has 4 filters with window length n, ($n \in \{3, 5, 7, 9, 16, 32, 64\}$). BN and MP stands for Batch Normalization and Max Pooling, respectively.

Figure 3.3: Proposed network architecture

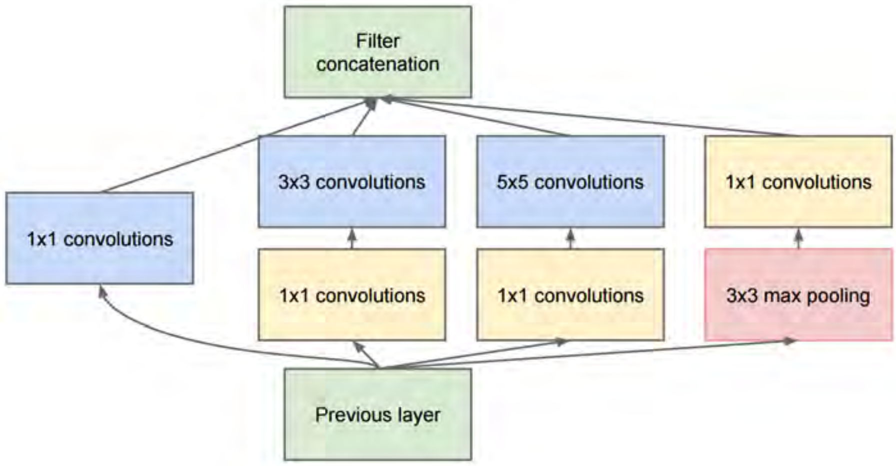

Figure 3.4: Inception module used in GoogleNet

In the popular neural network architecture GoogleNet [36], researchers have used varying window size in the same layer allowing it to look at image patches of different size. As shown in fig. 3.4, filters of varying kernel size is utilized at the same depth. A concatenation of different filter outputs are propagated to the next layer. This allows the network to learn the features from different filter size while training on the data. Inspired by this architecture we have used different window length for each of the convolution layers in the seven parallel paths. There are 4 filters in each path and the filter size vary from 3 to 64 as shown in fig 3.3b. This enables the inception block to look at the ECG signal at multiple spatial resolutions and extract multi-level features from the same input. The convolutional filters are gradually shifted by one sample and the input signal is zero padded to keep the output length unaltered (196 samples).

Batch Normalization Layer

The distribution of the output of the convolutional layer changes as the training parameters changes. The following layers have to continuously adapt to new distributions which requires it to have a slow learning rate. This phenomenon is referred to as *internal covariate shift* [38]. To tackle this issue a batch normalization layer is included after the convolutional layer. This layer includes a normalization step that fixes the means and variances of the following layer inputs (Algorithm 1).

Algorithm 1: Algorithm for batch normalization layer.

Input : Values of x over a mini-batch: $\mathcal{B} = \{x_{1...m}\}$;
Parameters to be learned: γ, β

Output: $\{y_i = BN_{\gamma,\beta}(x_i)\}$

$\mu_\beta \leftarrow \frac{1}{m}\sum_{i=1}^{m} x_i$ `// mini-batch mean`

$\sigma_\beta^2 \leftarrow \frac{1}{m}\sum_{i=1}^{m} (x_i - \mu_\beta)^2$ `// mini-batch variance`

$\hat{x}_i \leftarrow \frac{x_i - \mu_\beta}{\sqrt{\sigma_\beta^2 + \epsilon}}$ `// normalize`

$y_i \leftarrow \gamma\hat{x}_i + \beta \equiv BN_{\gamma,\beta}(x_i)$ `// scale and shift`

As a result, a higher learning rate can be used resulting in faster training time. Batch normalization layer also works as a regularizer [38].

ReLU layer

The rectified linear [39] layer induces a nonlinearity in the values of the incoming layer. The function of ReLU can be summarized mathematically as

$$f(x) = \begin{cases} x & \text{if } x > 0 \\ 0 & \text{if } x \leq 0 \end{cases} \tag{3.1}$$

i.e. it only passes the values x which are greater than zero. Other functions are also used to increase non-linearity, for example the saturating hyperbolic tangent $f(x) = tanh(x)$, $f(x) = |tanh(x)|$, and the sigmoid function $f(x) = \frac{1}{1+e^{-x}}$. ReLU is often preferred to other functions, because it trains the neural network several times faster without a significant penalty to generalization accuracy.

Max Pooling Layer

Max-pooling is useful in vision for two reasons:

- By eliminating non-maximal values, it reduces computation for upper layers.
- It provides a form of translation invariance.

The max pooling layer downsamples the input. This reduces computational cost due to the decrease in dimension and provides translational invariance to the internal representation. In our model, both the size of the pooling window and its stride was chosen to be two samples.

Global Average Pooling Layer

In traditional CNN's, convolutional layers are followed by dense layers which transform the feature maps into the desired output. However, the dense layers act as black-boxes which make it difficult to interpret the connection between filters and categorical outputs. Additionally, dense layers are prone to overfitting and computationally expensive due to its large number of parameters [40]. Hence, global average pooling layer is used which calculates the spatial average of each feature map. It summarizes the feature map extracted by each filter into a single value without the need of learning any parameters. As a result, we get 84 features from 84 filters which are passed on to the dense layer for classification.

3.2.4 IMI Detection

The two neurons of the output layer represents the probability of the input sample belonging to the IMI class and the HC class. The training progress of the CNN can be measured by different types of loss functions. Various loss functions appropriate for different tasks can be used in this layer. Softmax loss is used for predicting a single class of K mutually exclusive classes. Sigmoid cross-entropy loss is used for predicting K independent probability values in [0, 1]. Euclidean loss is used for regressing to real-valued labels $(-\inf, \inf)$. In this network we are using a softmax function applied to a categorical crossentropy loss function. For a 2 class problem the crossentropy is given by

$$\mathcal{L}(p, y) = -ylog(p) - (1-y)log(1-p) \tag{3.2}$$

Here, $y \in \{0, 1\}$ represents the true labels of each sample and p is the probability given by the model. The softmax output for each of the category is given by

$$\sigma_j = \frac{e^{L_j}}{\sum_{k=1}^{2} e^{L_k}}, \quad j \in \{1, 2\} \tag{3.3}$$

3.2.5 Prediction of Effective Lead combination for IMI Detection

To find the most effective lead combination in detecting IMI, nine leads, lead I, II, III, AVL, AVF, V1, V2, V3, and V4 are considered. Groups of three leads are chosen from these set of leads which resulted in 84 combinations. These groups include lead combinations capturing ST segment elevations only (1.19%), combinations capturing ST segment depressions only (11.90%) and combinations capturing both elevation and depression (86.91%). Features from these lead combinations are extracted using both the CNN and the SWT based method and its quality (defined in Chapter 4) is measured to make a comparison. Each lead combination is also used to train and test the model using a subject oriented approach.

3.3 Conclusion

In this Chapter we have described the filters used to preprocess the ECG signals. We have described the details of the network architecture, the motivations behind choosing a shallow but wide network and the procedure of measuring the network's performance. Also we have described the methodology to predict the most effective lead combination.

Chapter 4

Simulation Results

4.1 Introduction

In this chapter, the data description and the simulation parameters are presented. The training method of the proposed CNN is also explained in details. As mentioned before in subsection 3.2.3, the global average pooling layer compresses each incoming filter map into a single feature. Therefore, the output of the global average pooling layer can be considered as the final feature vector upon which the dense output layer makes its classification decision. We define two indices, Geometric Separability Index and Euclidean Distance in this section which are used to measure the quality of these features. To evaluate the model's performance a few metrics have been defined and compared with the benchmark model. Additionally, the result analysis is performed in this Chapter.

4.2 Data

The Physikalisch-Technische Bundesanstalt (PTB) dataset [41] collected from PhysioNet [42] were used in this work. The ECGs in this collection were obtained using a non-commercial, PTB prototype recorder with the following specifications:

- 16 input channels, (14 for ECGs, 1 for respiration, 1 for line voltage)
- Input voltage: ± 16 mV, compensated offset voltage up to ± 300 mV
- Input resistance: 100Ω (DC)
- Resolution: 16 bit with 0.5 μV/LSB (2000 A/D units per mV)
- Bandwidth: 0 - 1 kHz (synchronous sampling of all channels)

- Noise voltage: max. 10 μV (pp), respectively 3 μV (RMS) with input short circuit
- Online recording of skin resistance
- Noise level recording during signal collection

The database contains 549 records from 290 subjects (aged 17 to 87, mean 57.2; 209 men, mean age 55.5, and 81 women, mean age 61.6; ages were not recorded for 1 female and 14 male subjects). Each subject is represented by one to five records. There are no subjects numbered 124, 132, 134, or 161. Each record includes 15 simultaneously measured signals: the conventional 12 leads (i, ii, iii, avr, avl, avf, v1, v2, v3, v4, v5, v6) together with the 3 Frank lead ECGs (vx, vy, vz). Each signal is digitized at 1000 samples per second, with 16 bit resolution over a range of $\pm$16.384 mV. On special request to the contributors of the database, recordings may be available at sampling rates up to 10 KHz.

Within the header (.hea) file of most of these ECG records is a detailed clinical summary, including age, gender, diagnosis, and where applicable, data on medical history, medication and interventions, coronary artery pathology, ventriculography, echocardiography, and hemodynamics. The clinical summary is not available for 22 subjects. The diagnostic classes of the remaining 268 subjects are summarized below: There are 148 MI subjects and 52 healthy controls (HC). Thirty of the 148

Diagnostic class	**Number of subjects**
Myocardial infarction	148
Cardiomyopathy/Heart failure	18
Bundle branch block	15
Dysrhythmia	14
Myocardial hypertrophy	7
Valvular heart disease	6
Myocarditis	4
Miscellaneous	4
Healthy controls	52

Table 4.1: Number of diagnostic classes in the database.

MI patients have IMI; they are included in the experiment along with the healthy controls, resulting in a total of 82 subjects. Each subject is represented by one to five records.

4.3 Train-Test Split

Splitting of the train and test set is performed in a subject-oriented approach. In this approach the segments are grouped according to patients. Testing is done on one patient and training is done on the remaining 81 patients. The same procedure is followed for each of the 82 patients. Average accuracy, sensitivity and specificity of all the folds is reported in this thesis.

4.4 Data Preprocessing Parameters

The local window size of the median filters for the first and second stage is chosen to be 125 and 249 respectively. The SG filter had order 3 and frame size 15. After the segmentation of ECG signals 3222 IMI samples and 3055 HC samples are created.

4.5 Network Parameters

The CNN is implemented using Keras [43] neural network library which is a wrapper for the tensorflow machine learning framework [44]. The weights of the dense hidden layer are regularized using l2 regularization with regularization parameter $\lambda = 0.001$ to prevent the model from overfitting. The network is trained using the backpropagation algorithm [45]. The adam [46] optimizer is used to update the weights. The network is trained with an initial learning rate of 1e-3 and varied in the range [1e-3, 1e-5]. The exponential decay rate for the first moment estimates β_1 and the exponential decay rate for the second-moment estimates β_2 is chosen to be 0.9 and 0.999, respectively. The learning rate is scheduled to be decreased by a factor of 10 if there are no improvements in training loss for 5 consecutive epochs. Training is stopped if there is no improvement in training loss for 10 consecutive epochs. Training is allowed to run for a maximum of 200 epochs. The network is trained in mini-batches with batch size 32.

4.6 Geometric Separability Index

We use Thornton's geometric separability index (GSI) [47] to measure the degree to which samples associated with the same output cluster together. It is given by

$$GSI(f) = \frac{\sum_{i=1}^{N} f(\mathbf{x}_i) + f(\mathbf{x}_i^{'}) + 1 \ mod \ 2}{N} \tag{4.1}$$

Here, $\mathbf{x}_i = \{x_i^1, x_i^2, ..., x_i^L\}$ is the feature vector with dimension L, $\mathbf{x}_i^{'}$ is the nearest neighbor of $\mathbf{x}_i$, f is a binary target function, and N is the total number of samples. In this work, the nearest neighbor function utilizes Euclidean distance between a pair of feature vectors.

4.7 Euclidean Distance

To find out the similarity between features of the same class, we calculate the average of the euclidean distance (D_E^k) between each pair of samples within the same class.

$$D_E^k = \frac{(|\mathcal{N}_k| - 2)!2!}{|\mathcal{N}_k|!} \sum_{\substack{\mathbf{x}_i, \mathbf{x}_j \in \mathcal{N}_k \\ i \neq j}} \sqrt{\sum_{l=1}^{L} (x_i^l - x_j^l)^2} \tag{4.2}$$

Here, $\mathcal{N}_k$ is the set of feature vectors belonging to class k, $k \in \{HC, IMI\}$.

4.8 Comparison Metrics and Comparison Methods

The performance of the model was evaluated in terms of accuracy (Ac), sensitivity (Se), and specificity (Sp) of the test predictions. The metrics are defined as

$$Ac\% = \frac{tp + tn}{tp + tn + fp + fn} * 100 \tag{4.3}$$

$$Se\% = \frac{tp}{tp + fn} * 100 \tag{4.4}$$

$$Sp\% = \frac{tn}{tn + fp} * 100 \tag{4.5}$$

Here, tp is true positive prediction, fp is false positive prediction, tn is true negative prediction and fp is false negative prediction.

We compare the performance of our proposed method with the benchmark method [27]. In this method, the stationary wavelet transform is applied to the

ECG signals and the transform coefficients are used to calculate different features (e.g., sample entropy, energy etc.). These features are fed to a support vector machine (SVM) and K-nearest neighbour (KNN) classifier to perform IMI detection.

4.9 Result Analysis

4.9.1 Quality of Features Extracted from Reference Lead Combination

First, we compare the quality of features extracted from the reference lead combination using CNN and SWT method. Euclidean distance of features and GSI are calculated for both the proposed model and benchmark model. We implement the stationary wavelet transform based model [27] and compute the features for each sample. To extract the feature using CNN, we train our network on all of the available samples. For each of the samples, the output of the global average pooling layer is extracted and treated as the feature vector. The confusion matrix for the training performance of the model is shown in Table 4.2.

Table 4.2: Confusion matrix for the CNN's prediction when trained on all the patients

		Predicted Class	
		HC	IMI
Actual Class	HC	2833	222
	IMI	10	3212

The GSI and D_E^k of the proposed and benchmark model is compared in Table 4.3. The GSI is high for both models, signifying that the feature vectors of the same class are located in a close cluster. The GSI of the proposed model is greater than the GSI of the benchmark. For the healthy samples, the D_E^{HC} of the proposed model is slightly greater than the benchmark model. For the IMI samples, the D_E^{IMI} of the proposed model is lower than the benchmark model. Overall, the features extracted from the proposed model shows good discriminating strength.

Table 4.3: Comparison of D_E^k between benchmark and proposed model

Method	GSI	D_E^{HC}	D_E^{IMI}
SWT	0.9852	3.10	3.71
CNN	0.9986	3.54	2.94

4.9.2 Metrics Results on Reference Combination

Next, we compare the performance of the benchmark and the proposed model on the reference lead combination in terms of the metrics defined earlier. The proposed model is trained and tested according to the subject-oriented method described in 4.3. The metrics scores for the proposed CNN and the benchmark method is summarized in Table 4.4. The proposed method outscores the benchmark method in all the metrics.

Table 4.4: Comparison of the proposed technique with existing method in subject-oriented approach

Method	Ac%	Se%	Sp%
SWT + KNN [27]	75.80	75.62	73.66
SWT + SVM [27]	81.71	79.01	79.26
CNN on raw ECG	85.45	85.79	85.25

4.9.3 Quality of Feature of Different Lead Combinations

Next, to predict the most effective lead combination in detecting IMI, the quality of feature was measured for each of the lead groups defined in subsection 3.2.5. Each of the lead combinations is assigned a number for brevity which is listed in Table 4.5. Variation of average Euclidean distance, GSI, along with different leads is shown in Fig. 4.1 to 4.3. These figures also show the performance of the benchmark SWT based methods performance along with the CNN's performance.

It can be seen that the Euclidean distances are better in case of the lead combinations which has a mixture of leads capturing ST segment elevation and depression. In Fig. 4.1, the variation of average Euclidean distance D_E^{HC} of the features extracted from the healthy samples for different lead combinations is shown. Here, D_E^{HC} of lead I, II, V4 is lowest. In Fig. 4.2, the variation of average Euclidean distance D_E^{IMI} of the features extracted from the healthy samples for different lead combinations is shown and lead II, AVF, V2 has the lowest D_E^{IMI}. In the case of the GSI (Fig. 4.3), lead AVL, V1, and V3 scores the highest value. Although these leads capture only the ST segment depression, all other lead combinations show a good performance remaining close to the highest value and performs much better than the SWT method.

Table 4.5: Assigned numbers to the lead combinations

Leads	No.	Leads	No.	Leads	No.
(I, II, III)	0	(II, III, AVL)	28	(III, AVF, V3)	56
(I, II, AVL)	1	(II, III, AVF)	29	(III, AVF, V4)	57
(I, II, AVF)	2	(II, III, V1)	30	(III, V1, V2)	58
(I, II, V1)	3	(II, III, V2)	31	(III, V1, V3)	59
(I, II, V2)	4	(II, III, V3)	32	(III, V1, V4)	60
(I, II, V3)	5	(II, III, V4)	33	(III, V2, V3)	61
(I, II, V4)	6	(II, AVL, AVF)	34	(III, V2, V4)	62
(I, III, AVL)	7	(II, AVL, V1)	35	(III, V3, V4)	63
(I, III, AVF)	8	(II, AVL, V2)	36	(AVL, AVF, V1)	64
(I, III, V1)	9	(II, AVL, V3)	37	(AVL, AVF, V2)	65
(I, III, V2)	10	(II, AVL, V4)	38	(AVL, AVF, V3)	66
(I, III, V3)	11	(II, AVF, V1)	39	(AVL, AVF, V4)	67
(I, III, V4)	12	(II, AVF, V2)	40	(AVL, V1, V2)	68
(I, AVL, AVF)	13	(II, AVF, V3)	41	(AVL, V1, V3)	69
(I, AVL, V1)	14	(II, AVF, V4)	42	(AVL, V1, V4)	70
(I, AVL, V2)	15	(II, V1, V2)	43	(AVL, V2, V3)	71
(I, AVL, V3)	16	(II, V1, V3)	44	(AVL, V2, V4)	72
(I, AVL, V4)	17	(II, V1, V4)	45	(AVL, V3, V4)	73
(I, AVF, V1)	18	(II, V2, V3)	46	(AVF, V1, V2)	74
(I, AVF, V2)	19	(II, V2, V4)	47	(AVF, V1, V3)	75
(I, AVF, V3)	20	(II, V3, V4)	48	(AVF, V1, V4)	76
(I, AVF, V4)	21	(III, AVL, AVF)	49	(AVF, V2, V3)	77
(I, V1, V2)	22	(III, AVL, V1)	50	(AVF, V2, V4)	78
(I, V1, V3)	23	(III, AVL, V2)	51	(AVF, V3, V4)	79
(I, V1, V4)	24	(III, AVL, V3)	52	(V1, V2, V3)	80
(I, V2, V3)	25	(III, AVL, V4)	53	(V1, V2, V4)	81
(I, V2, V4)	26	(III, AVF, V1)	54	(V1, V3, V4)	82
(I, V3, V4)	27	(III, AVF, V2)	55	(V2, V3, V4)	83

4.9.4 Metrics Scores for Different Lead Combinations

Finally, each of the lead combinations is used to train and test the proposed model in a subject oriented approach and its performance metrics are calculated. Variation of accuracy, sensitivity, and specificity along with different leads are shown in Fig. 4.4 to 4.6. Also, the metrics scores in SWT method is included for comparison. In Fig. 4.4 accuracy of the different lead combination is shown where lead II, III, V1 shows the highest accuracy. In case of sensitivity, Fig. 4.5, lead II, III, V3 scores the highest value. In Fig. 4.6, lead II, III, V3 shows the highest specificity. Each of these combinations contains leads which capture both ST segment elevation and depression and outperforms combination of lead II, III, and AVF.

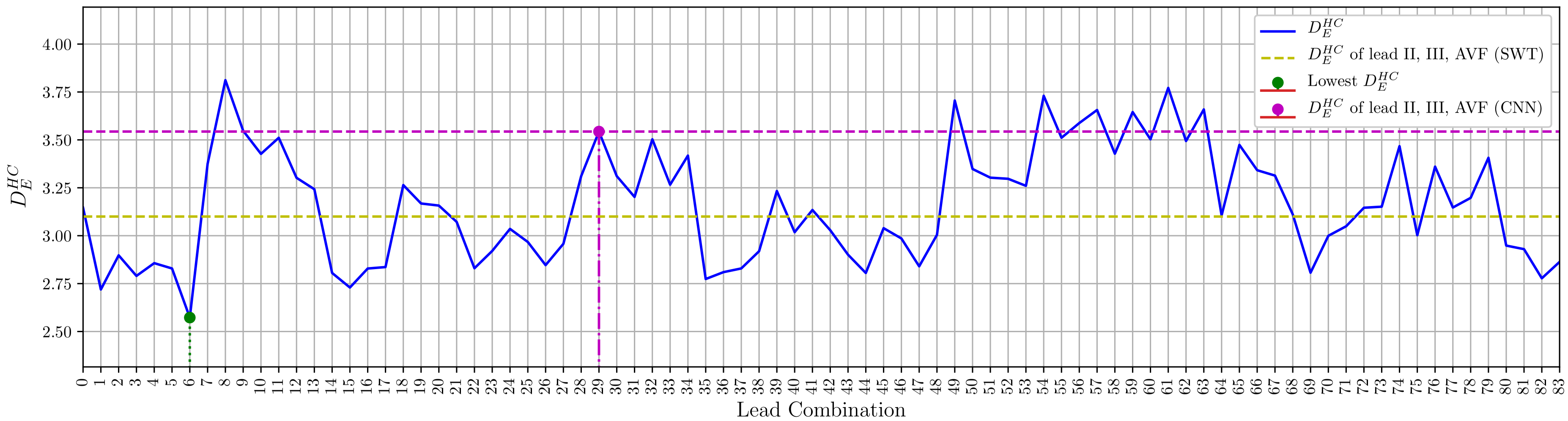

Figure 4.1: Variation of Euclidean distance of HC class (D_E^{HC}) with lead combinations

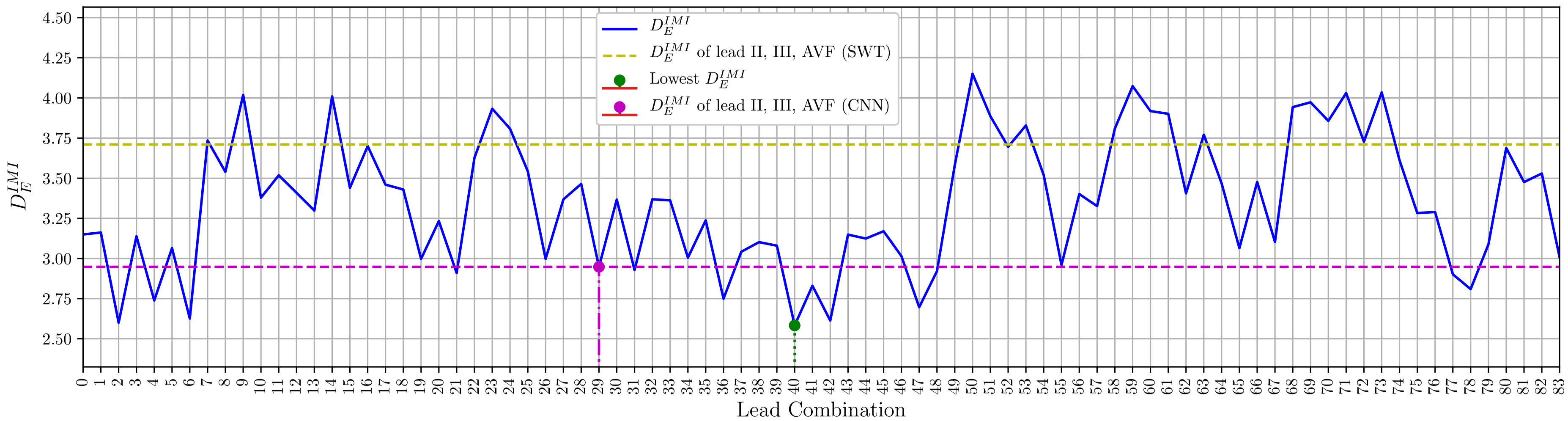

Figure 4.2: Variation of Euclidean distance of IMI (D_E^{IMI}) with lead combinations

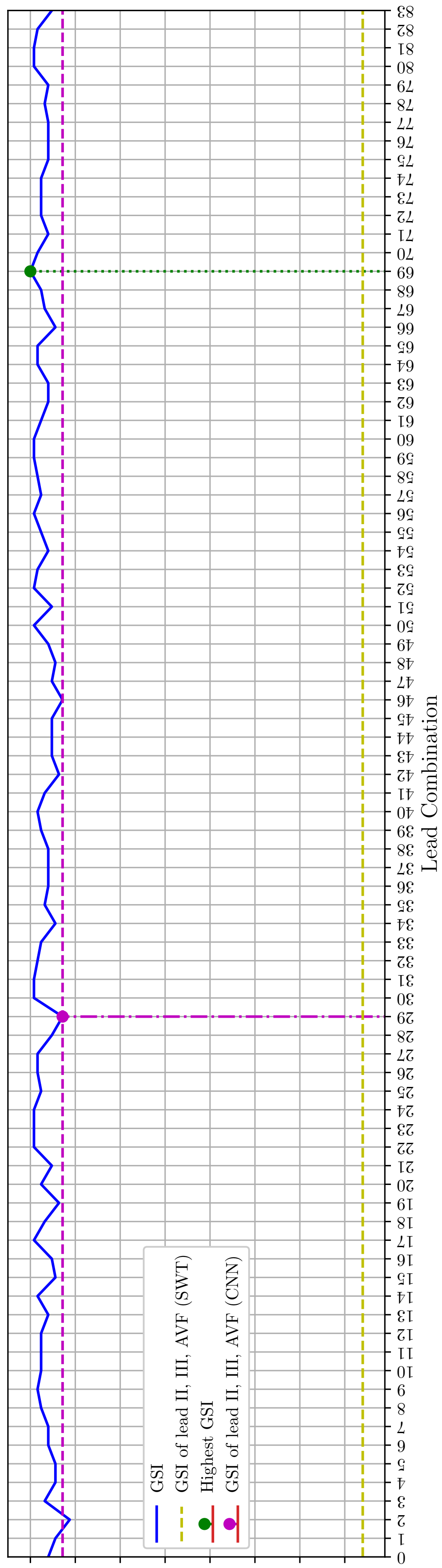

Figure 4.3: Variation of GSI with lead combinations

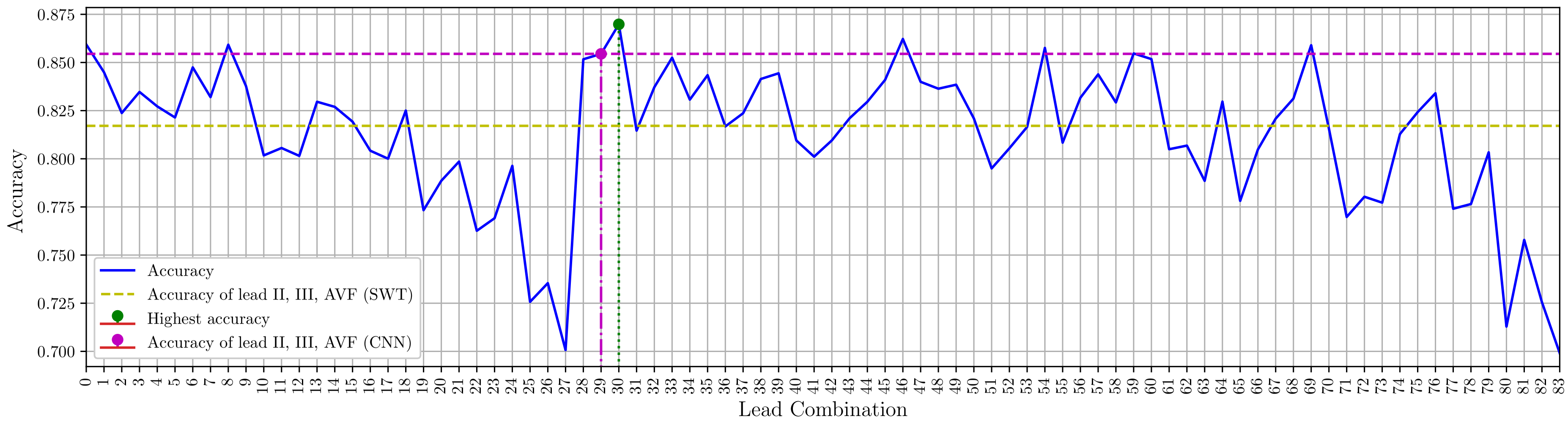

Figure 4.4: Variation of accuracy with lead combinations

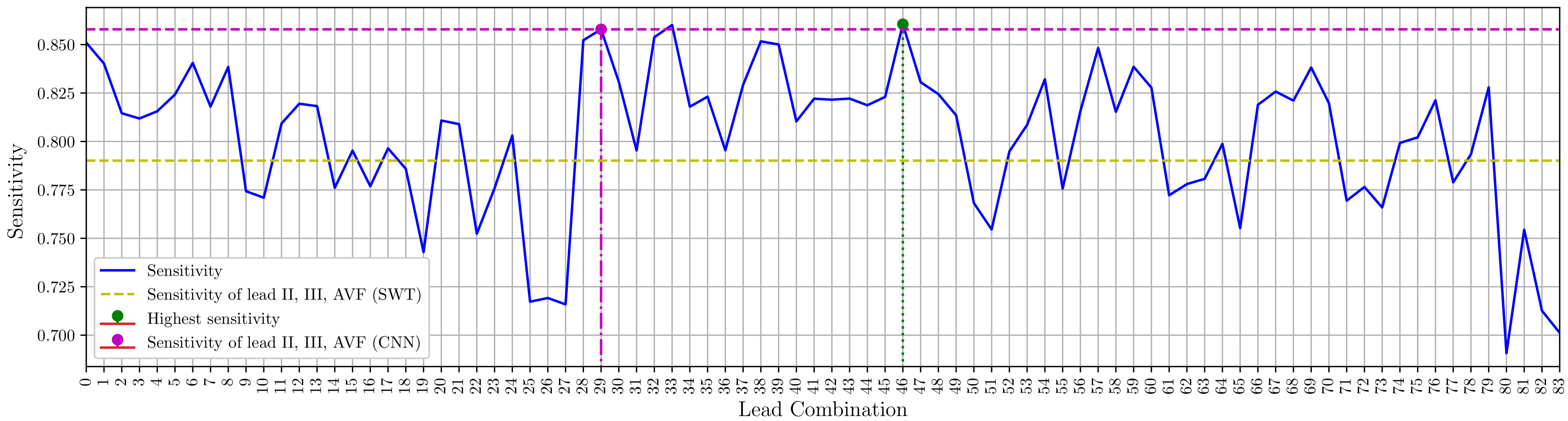

Figure 4.5: Variation of sensitivity with lead combinations.

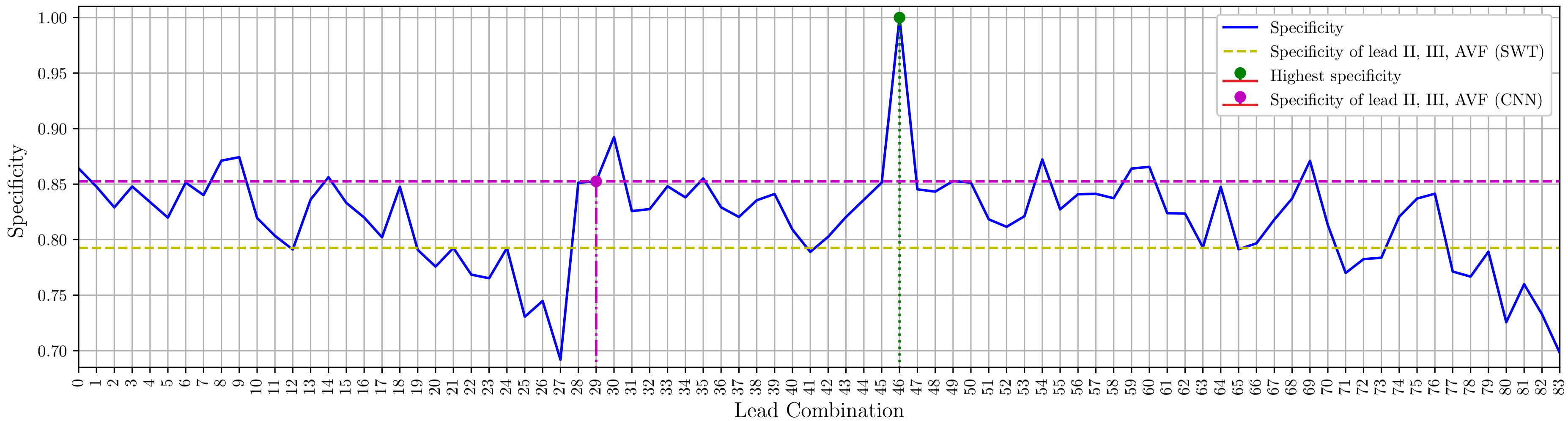

Figure 4.6: Variation of specificity with lead combinations

4.9.5 Finding Most Effective Lead Combination

Overall, the features extracted from lead combination II, III, V3 have better quality in terms of the Euclidean distances (D_E^{HC}=2.99, D_E^{IMI}= 3.02) which is lower than the distances of the reference lead combination. Additionally, GSI of both the combinations are equal (0.9986). However, the better euclidean distances results in a better metrics score for the former combination as it outperforms the reference lead combination in every metric with an accuracy, sensitivity, and specificity of 86.22%, 86.05%, and 100% respectively (Table 4.6). Since lead II, III captures ST segment elevation and V3 captures ST segment depression, this shows the importance of focusing on both ST segment elevation and depression while detecting IMI.

Table 4.6: Comparison of the quality of features and metrics scores between reference lead combination and combination of lead II, III, and V3

Leads	Quality of features			Comparison Metrics		
	D_E^{HC}	D_E^{IMI}	GSI	Ac%	Se%	Sp%
II, III, AVF	3.54	2.94	0.9986	85.45	85.79	85.25
II, III, V3	2.99	3.02	0.9986	86.22	86.05	100

4.10 Conclusion

In this Chapter, we have presented the simulation details and result analysis. The proposed method based on shallow CNN outperforms the benchmark model. The lead II, III, and V3 is the most effective lead combination in detecting IMI. Additionally, the quality of features extracted using the CNN and SWT based method concur with the observed performance in metrics score.

Chapter 5

CONCLUSION

5.1 Concluding Remarks

In this thesis, we have demonstrated the use of a shallow convolutional neural network in the detection of inferior myocardial infarction. This network benefits from the use of varying filter size in the same convolution layer which allows it to learn features from signal regions of varying length. The model outperforms the previous state of the art model in terms of accuracy, sensitivity, and specificity. We have also made a comparison among different lead combinations and found out that the combination of leads that capture ST segment elevation and ST segment depression is more effective in distinguishing IMI from healthy patients.

5.2 Contribution

- We developed an end to end system to detect IMI from raw ECG signal and compare its performance with the state of the art feature based method which uses a stationary wavelet based method (SWT).
- We designed a shallow but wide CNN with less number of parameters compared to traditional deep CNNs
- We evaluated the performance of the shallow CNN in a leave-one-patient-out (subject-oriented) approach and to make a qualitative comparison between features extracted by the shallow CNN and the hand engineered features based model.
- We investigated the predictive capability of different lead combinations which considers not only ST segment elevation but also ST segment depression.

5.3 Future Research

There are a wide range of areas yet to be explored.

- Future research should focus on the effect of varying the filter length as well as increasing the number of inception layers.
- Another important research direction is the study of the relationship between the extracted features and the actual ECG segments. Finding out which portions of the ECG signal activate the filters would lead to a better understanding of the disease itself.
- And lastly this research only focuses on the detection of inferior myocardial infarction. Classification of different infarctions based on their positions should be investigated in future works.

Bibliography

[1] E. J. Benjamin, M. J. Blaha, S. E. Chiuve, M. Cushman, S. R. Das, R. Deo, S. D. de Ferranti, J. Floyd, M. Fornage, C. Gillespie *et al.*, "Heart disease and stroke statistics-2017 update: a report from the American Heart Association," *Circulation*, vol. 135, no. 10, pp. e146–e603, 2017.

[2] E. Antman, J.-P. Bassand, W. Klein, M. Ohman, J. L. L. Sendon, L. Rydén, M. Simoons, and M. Tendera, "Myocardial infarction redefined—a consensus document of The Joint European Society of Cardiology/American College of Cardiology committee for the redefinition of myocardial infarction: The Joint European Society of Cardiology/American College of Cardiology Committee∗∗ A list of contributors to this ESC/ACC Consensus Document is provided in Appendix B." *Journal of the American College of Cardiology*, vol. 36, no. 3, pp. 959–969, 2000.

[3] S. M. Salerno, P. C. Alguire, and H. S. Waxman, "Competency in interpretation of 12-lead electrocardiograms: a summary and appraisal of published evidence," *Annals of Internal Medicine*, vol. 138, no. 9, pp. 751–760, 2003.

[4] M. J. Warner and S. S. Bhimji, "Myocardial Infarction, Inferior," 2017.

[5] J. R. Salcedo, M. G. Baird, R. J. Chambers, and D. S. Beanlands, "Significance of reciprocal ST segment depression in anterior precordial leads in acute inferior myocardial infarction: concomitant left anterior descending coronary artery disease," *The American journal of cardiology*, vol. 48, no. 6, pp. 1003–1008, 1981.

[6] B. C. Csáji, "Approximation with artificial neural networks," *Faculty of Sciences, Etvs Lornd University, Hungary*, vol. 24, p. 48, 2001.

[7] A. Krizhevsky, I. Sutskever, and G. E. Hinton, "Imagenet classification with deep convolutional neural networks," in *Advances in Neural Information Processing Systems*, 2012, pp. 1097–1105.

[8] K. Simonyan and A. Zisserman, "Very deep convolutional networks for large-scale image recognition," *arXiv preprint arXiv:1409.1556*, 2014.

[9] K. He, X. Zhang, S. Ren, and J. Sun, "Deep residual learning for image recognition," in *Proceedings of the IEEE conference on computer vision and pattern recognition*, 2016, pp. 770–778.

[10] S. Bell and K. Bala, "Learning visual similarity for product design with convolutional neural networks," *ACM Transactions on Graphics (TOG)*, vol. 34, no. 4, p. 98, 2015.

[11] S. Ren, K. He, R. Girshick, and J. Sun, "Faster r-cnn: Towards real-time object detection with region proposal networks," in *Advances in Neural Information Processing Systems*, 2015, pp. 91–99.

[12] J. Redmon, S. Divvala, R. Girshick, and A. Farhadi, "You only look once: Unified, real-time object detection," in *Proceedings of the IEEE conference on computer vision and pattern recognition*, 2016, pp. 779–788.

[13] O. Ronneberger, P. Fischer, and T. Brox, "U-net: Convolutional networks for biomedical image segmentation," in *International Conference on Medical image computing and computer-assisted intervention.* Springer, 2015, pp. 234–241.

[14] K. He, G. Gkioxari, P. Dollár, and R. Girshick, "Mask r-cnn," in *IEEE International Conference on Computer Vision (ICCV)*, 2017, pp. 2980–2988.

[15] J. Long, E. Shelhamer, and T. Darrell, "Fully convolutional networks for semantic segmentation," in *Proceedings of the IEEE conference on computer vision and pattern recognition*, 2015, pp. 3431–3440.

[16] P. Rajpurkar, A. Y. Hannun, M. Haghpanahi, C. Bourn, and A. Y. Ng, "Cardiologist-Level Arrhythmia Detection with Convolutional Neural Networks," *arXiv preprint arXiv:1707.01836*, 2017.

[17] U. R. Acharya, H. Fujita, O. S. Lih, M. Adam, J. H. Tan, and C. K. Chua, “Automated detection of coronary artery disease using different durations of ECG segments with convolutional neural network,” *Knowledge-Based Systems*, vol. 132, pp. 62–71, 2017.

[18] S. Kiranyaz, T. Ince, and M. Gabbouj, “Real-time patient-specific ECG classification by 1-D convolutional neural networks,” *IEEE Transactions on Biomedical Engineering*, vol. 63, no. 3, pp. 664–675, 2016.

[19] M. Zubair, J. Kim, and C. Yoon, “An automated ECG beat classification system using convolutional neural networks,” in *6th International Conference on IT Convergence and Security (ICITCS)*, 2016, pp. 1–5.

[20] L. Zhou, Y. Yan, X. Qin, C. Yuan, D. Que, and L. Wang, “Deep learning-based classification of massive electrocardiography data,” in *Advanced Information Management, Communicates, Electronic and Automation Control Conference (IMCEC)*, 2016, pp. 780–785.

[21] Q. Zhang, D. Zhou, and X. Zeng, “HeartID: a multiresolution convolutional neural network for ECG-based biometric human identification in smart health applications,” *IEEE Access*, vol. 5, pp. 11 805–11 816, 2017.

[22] B. Taji, A. D. Chan, and S. Shirmohammadi, “Classifying measured electrocardiogram signal quality using deep belief networks,” in *IEEE International Instrumentation and Measurement Technology Conference (I2MTC)*, 2017, pp. 1–6.

[23] C. Zhang, G. Wang, J. Zhao, P. Gao, J. Lin, and H. Yang, “Patient-specific ECG classification based on recurrent neural networks and clustering technique,” in *13th IASTED International Conference on Biomedical Engineering (BioMed)*, 2017, pp. 63–67.

[24] M. Cheng, W. J. Sori, F. Jiang, A. Khan, and S. Liu, “Recurrent Neural Network Based Classification of ECG Signal Features for Obstruction of Sleep Apnea Detection,” in *IEEE International Conference on Computational Science and Engineering (CSE) and Embedded and Ubiquitous Computing (EUC)*, vol. 2, 2017, pp. 199–202.

[25] R. Salloum and C.-C. J. Kuo, "ECG-based biometrics using recurrent neural networks," in *IEEE International Conference on Acoustics, Speech and Signal Processing (ICASSP)*, 2017, pp. 2062–2066.

[26] U. R. Acharya, H. Fujita, V. K. Sudarshan, S. L. Oh, M. Adam, J. E. Koh, J. H. Tan, D. N. Ghista, R. J. Martis, C. K. Chua *et al.*, "Automated detection and localization of myocardial infarction using electrocardiogram: a comparative study of different leads," *Knowledge-Based Systems*, vol. 99, pp. 146–156, 2016.

[27] L. D. Sharma and R. K. Sunkaria, "Inferior myocardial infarction detection using stationary wavelet transform and machine learning approach," *Signal, Image and Video Processing*, pp. 1–8, 2017.

[28] J. Wu, Y. Bao, S.-C. Chan, H. Wu, L. Zhang, and X.-G. Wei, "Myocardial infarction detection and classification—A new multi-scale deep feature learning approach," in *IEEE International Conference on Digital Signal Processing (DSP)*, 2016, pp. 309–313.

[29] M. Arif, I. A. Malagore, and F. A. Afsar, "Detection and localization of myocardial infarction using k-nearest neighbor classifier," *Journal of Medical Systems*, vol. 36, no. 1, pp. 279–289, 2012.

[30] B. Liu, J. Liu, G. Wang, K. Huang, F. Li, Y. Zheng, Y. Luo, and F. Zhou, "A novel electrocardiogram parameterization algorithm and its application in myocardial infarction detection," *Computers in Biology and Medicine*, vol. 61, pp. 178–184, 2015.

[31] P.-C. Chang, J.-J. Lin, J.-C. Hsieh, and J. Weng, "Myocardial infarction classification with multi-lead ECG using hidden Markov models and Gaussian mixture models," *Applied Soft Computing*, vol. 12, no. 10, pp. 3165–3175, 2012.

[32] R. Tripathy and S. Dandapat, "Detection of myocardial infarction from vectorcardiogram using relevance vector machine," *Signal, Image and Video Processing*, pp. 1–8, 2017.

[33] B. Hedén, H. Ohlin, R. Rittner, and L. Edenbrandt, "Acute myocardial infarction detected in the 12-lead ECG by artificial neural networks." *Circulation*, vol. 96, no. 6, pp. 1798–1802, 1997.

[34] H. Haraldsson, L. Edenbrandt, and M. Ohlsson, "Detecting acute myocardial infarction in the 12-lead ECG using Hermite expansions and neural networks," *Artificial Intelligence in Medicine*, vol. 32, no. 2, pp. 127–136, 2004.

[35] U. R. Acharya, H. Fujita, S. L. Oh, Y. Hagiwara, J. H. Tan, and M. Adam, "Application of deep convolutional neural network for automated detection of myocardial infarction using ECG signals," *Information Sciences*, vol. 415, pp. 190–198, 2017.

[36] C. Szegedy, W. Liu, Y. Jia, P. Sermanet, S. Reed, D. Anguelov, D. Erhan, V. Vanhoucke, and A. Rabinovich, "Going deeper with convolutions," in *Proceedings of the IEEE conference on computer vision and pattern recognition*, 2015, pp. 1–9.

[37] A. Krizhevsky, I. Sutskever, and G. E. Hinton, "Imagenet classification with deep convolutional neural networks," in *Advances in Neural Information Processing Systems*, 2012, pp. 1097–1105.

[38] S. Ioffe and C. Szegedy, "Batch normalization: Accelerating deep network training by reducing internal covariate shift," in *International Conference on Machine Learning*, 2015, pp. 448–456.

[39] V. Nair and G. E. Hinton, "Rectified linear units improve restricted boltzmann machines," in *Proceedings of the 27th international conference on machine learning (ICML-10)*, 2010, pp. 807–814.

[40] M. Lin, Q. Chen, and S. Yan, "Network in network," *arXiv preprint arXiv:1312.4400*, 2013.

[41] R. Bousseljot, D. Kreiseler, and A. Schnabel, "Nutzung der EKG-Signaldatenbank CARDIODAT der PTB über das Internet," *Biomedizinische Technik/Biomedical Engineering*, vol. 40, no. s1, pp. 317–318, 1995.

[42] A. L. Goldberger, L. A. Amaral, L. Glass, J. M. Hausdorff, P. C. Ivanov, R. G. Mark, J. E. Mietus, G. B. Moody, C.-K. Peng, and H. E. Stanley, "Physiobank, physiotoolkit, and physionet," *Circulation*, vol. 101, no. 23, pp. e215–e220, 2000.

[43] F. Chollet *et al.*, "Keras," 2015.

[44] M. Abadi, A. Agarwal, P. Barham, E. Brevdo, Z. Chen, C. Citro, G. S. Corrado, A. Davis, J. Dean, M. Devin, S. Ghemawat, I. Goodfellow, A. Harp, G. Irving, M. Isard, Y. Jia, R. Jozefowicz, L. Kaiser, M. Kudlur, J. Levenberg, D. Mané, R. Monga, S. Moore, D. Murray, C. Olah, M. Schuster, J. Shlens, B. Steiner, I. Sutskever, K. Talwar, P. Tucker, V. Vanhoucke, V. Vasudevan, F. Viégas, O. Vinyals, P. Warden, M. Wattenberg, M. Wicke, Y. Yu, and X. Zheng, "TensorFlow: Large-Scale Machine Learning on Heterogeneous Systems," 2015, software available from tensorflow.org. [Online]. Available: https://www.tensorflow.org/

[45] Y. LeCun, Y. Bengio, and G. Hinton, "Deep learning," *nature*, vol. 521, no. 7553, p. 436, 2015.

[46] D. Kingma and J. Ba, "Adam: A method for stochastic optimization," *arXiv preprint arXiv:1412.6980*, 2014.

[47] C. Thornton, "Separability is a learner's best friend," in *4th Neural Computation and Psychology Workshop, London, 9–11 April 1997*. Springer, 1998, pp. 40–46.